Computing the Shallow Water Equations on a Sphere by Finite Volume Methods

Ragnhild Blikberg*
Dept. of Informatics/Parallab,
University of Bergen,
NORWAY

Tor Sørevik†
Dept. of Informatics,
University of Bergen,
NORWAY

February 19, 2003

Abstract

In this paper we report on our experiences applying the finite volume method to the shallow water equations on a sphere. The equations are based on spherical coordinates and discretized on a regular latitude-longitude grid.

We have applied our methods to problems from the standard test suite of Williamson et al. [WDH+91], the simplest of these being steady state problems. The standard wave-propagation method did not reproduce the steady state in these cases. However, a steady state solution was achieved by a flux-based wave propagation method with second order correction.

The great advantage of the finite volume technique is that it, by construction, gives conservation of mass and momentum. However, the classical problem of how to deal with the polar singularity when transforming the problem to spherical coordinates is very much present.

Keywords: Finite volume method, Shallow water equations, spherical coordinates, wave-propagation

*http://www.ii.uib.no/~ragnhild
†http://www.ii.uib.no/~tors

1 Introduction

The shallow water equations (SWE) is the simplest possible model that captures the essential features of fluid flow on the earth, and has for that reason become the standard test bed for numerical techniques. In order to evaluate and compare different schemes a standard test suite of seven problem was in 1992 proposed by Williamson et al. [WDH$^+$91]. This test suite has been widely accepted by the atmospheric modeling community. In a companion paper [JCHW95] a reference solution based on the spectral transform method is provided.

For long running simulations the conservation of mass and momentum are of great importance and techniques which render only small conservation losses in a five day run (= weather forecast) may give unacceptable losses in a fifty year run (= climate modeling). This stimulate us to look at finite volume discretization techniques as these methods are designed to be conservative. To minimize the coding effort our code has been built on CLAWPACK [LLBM00], a package which implements a wave propagating version of the finite volume method (FVM) for conservation laws.

In CLAWPACK the user must provide the decomposition of the fluxes into waves for solving the associated Riemann problem which emerge after approximating the state variables with cell centered averages. The standard technique is to work with the equations in the quasilinear advection form for this decomposition. Recently a new decomposition strategy where one works directly with the fluxes has been introduced [BLMR03]. Potential advantages of this method is that Roe's criteria [Roe81] for averaging the state variables at cell interfaces may be relaxed. Flux-based decomposition also gives an opportunity for the (partial) incorporation of source terms in the wave decomposition, and thereby avoiding any splitting error.

We have chosen to represent the equations in spherical coordinates and discretize the sphere using a regular latitude-longitude grid. This implies that we have to deal with the well known pole-problem: singularity in the derivatives, caused by the $1/\cos\theta$ term in the spherical formulation of the equations, degeneration of the rectangular cells to spherical triangles, artificial boundary conditions in the latitude direction, etc... The explicit singularity is avoided in our scheme as the state variables are represented at cell centers only, while the poles represent a (degenerated) cell interface. However, as the grid gets finer, one should expect the near singularities to cause great computational inaccuracy.

The simplest of the problems from the test suite in [WDH$^+$91] has analytical known solutions. These problems are all steady state problems. Although these problems are usually seen as simpler than real life problems they are not trivial. A particular problem for our method on these problems is related to the fact that they represent a steady state. In CLAWPACK a split operator technique is used when a source term appear in the equations. The splitting error is of the same order as other discretization errors and for that reason usually not considered any problem. However, when applied to steady state problems, the operator splitting solves two individual problems which each is far from steady state. To have a small overall error, two relative large ones have to cancel each other. This easily leads to small oscillations around the steady state. Our experiments shows that the flux-based wave decomposition is more robust in this respect.

This paper is organized as follows. First the equations are introduced in Section 2. Section 3 outlines how to compute the standard wave decomposition of quasi-linear advection form as well as the flux-based wave decomposition. The modification needed to obtain a higher order method will also be described. Section 4 contains a description of the grid we are using, and the numerical results are presented and discussed in Section 5. In Section 6 we discuss the advantages and disadvantaged of our approach in comparison with other methods. We also briefly discuss alternative grids. Plans for future work are sketched in Section 7.

2 The shallow water equations on a sphere

In spherical coordinates, where the longitudes are given by ϕ and the latitudes by θ, the SWE on a sphere can be written as

$$\mathbf{q}_t + \mathbf{f}_\phi + \mathbf{g}_\theta = \mathbf{s}. \tag{1}$$

The state variables are the depth, $h(\phi,\theta,t)$, the zonal velocity, $u(\phi,\theta,t)$ and the meridional velocity, $v(\phi,\theta,t)$. In these variables the vectors of (1) becomes

$$\mathbf{q} = \begin{pmatrix} h' \\ h'u \\ h'v \end{pmatrix}, \quad \mathbf{f} = \begin{pmatrix} \frac{h'u}{a\cos\theta} \\ \frac{h'u^2}{a\cos\theta} + \frac{h'^2 g}{2a\cos^2\theta} \\ \frac{h'uv}{a\cos\theta} \end{pmatrix}, \quad \mathbf{g} = \begin{pmatrix} \frac{h'v}{a} \\ \frac{h'uv}{a} \\ \frac{h'v^2}{a} + \frac{h'^2 g}{2a\cos\theta} \end{pmatrix}. \tag{2}$$

To eliminate a $\cos\theta$ term from the time derivative, the substitution $h' = h\cos\theta$ has been made. The Coriolis force is given by f. In the case of a flat topography the right hand side becomes

$$\mathbf{s} = \begin{pmatrix} 0 \\ \left(f + \frac{u\tan\theta}{a}\right) h'v \\ -\left(f + \frac{u\tan\theta}{a}\right) h'u - \frac{h'^2 g}{2a}\frac{\tan\theta}{\cos\theta} \end{pmatrix}. \tag{3}$$

Additional terms is needed in $\mathbf{s}$, if one needs to incorporate topography.

(1) can also be written in quasi-linear advection form as

$$\mathbf{q}_t + \mathbf{A}\mathbf{q}_\phi + \mathbf{B}\mathbf{q}_\theta = \mathbf{s} \tag{4}$$

where $\mathbf{A}$, the Jacobian of $\mathbf{f}$, is

$$\mathbf{A} = \frac{\partial \mathbf{f}}{\partial \mathbf{q}} = \frac{1}{a\cos\theta}\begin{pmatrix} 0 & 1 & 0 \\ -u^2 + hg & 2u & 0 \\ -uv & v & u \end{pmatrix}, \tag{5}$$

and $\mathbf{B}$, the Jacobian of $\mathbf{g}$, is

$$\mathbf{B} = \frac{\partial \mathbf{g}}{\partial \mathbf{q}} = \frac{1}{a}\begin{pmatrix} 0 & 0 & 1 \\ -uv & v & u \\ -v^2 + hg & 0 & 2v \end{pmatrix}. \tag{6}$$

3 Wave-propagation algorithms for SWE

For solving this problem we will discretize the sphere into regular cells and apply a finite volume technique using the CLAWPACK library [LLBM00]. For conservation laws with source term (also called balance laws), CLAWPACK applies an operator splitting technique. (1) is rewritten as:

$$\begin{aligned} \mathbf{q}_t^* + \mathbf{f}_\phi + \mathbf{g}_\theta &= \mathbf{0} \qquad (7) \\ \mathbf{q}_t &= \mathbf{s}(\mathbf{q}^*) \qquad (8) \end{aligned}$$

Here the last equation is a system of ODEs and can be solved by any standard ODE-solver while (7) is solved by a wave-propagation version of Godunov's method (or higher order correction of it). See [LeV02] for details.

In one space dimension, $q_t + f(q)_x = 0$, Godunov's method takes the simple form

$$Q_i^{n+1} = Q_i^n - \frac{\delta t}{\delta x}(F_{i+1/2}^n - F_{i-1/2}^n). \tag{9}$$

For a fixed point in time, t_n, the vector of conserved quantities, $q(x,t)$, is in each cell approximated by a cell average, Q_i^n.

$$Q_i^n \approx \frac{1}{\delta x}\int_{x_{i-1/2}}^{x_{i+1/2}} q(x,t_n)\,dx \tag{10}$$

while

$$F_{i\pm 1/2}^n \approx \frac{1}{\delta t}\int_{t_n}^{t_{n+1}} f(q(x_{i\pm 1/2},t))\,dt \tag{11}$$

is the approximation of the fluxes across cell interfaces.

In two dimensions fluxes are computed exactly the same way in the second direction too, and the total update over all four cell interfaces becomes

$$Q_{i,j}^{n+1} = Q_{i,j}^n - \frac{\delta t}{\delta x}(F_{i+1/2,j}^n - F_{i-1/2,j}^n) - \frac{\delta t}{\delta y}(G_{i,j+1/2}^n - G_{i,j-1/2}^n). \tag{12}$$

To keep the notation simple we will limit ourselves to only one spacial index in the reminder.

By approximating $q(x,t)$ by a piecewise constant function (10) we in each time step are faced with solving a Riemann problem. This allows us to decompose the fluxes at the cell interfaces into waves determined by the eigenvectors of the Jacobian (in the nonlinear case a local linear approximation). The contribution of the different waves is determined by the "jump" in values of neighboring cells. Below the details of two different ways of determining these waves are given. In the case where $\mathbf{f}$ is autonomous the two wave decompositions coincide, but in spherical coordinates that is not the case for the SWE.

3.1 Standard wave-propagation algorithm

3.1.1 Wave decomposition in the ϕ-direction

The eigendecomposition of $\mathbf{A}$ is

$$\begin{array}{rclcrcl}
\lambda^1 &=& \frac{u+\sqrt{hg}}{a\cos\theta}; && \mathbf{r}^1 &=& (1, u+\sqrt{hg}, v)^T \\
\lambda^2 &=& \frac{u-\sqrt{hg}}{a\cos\theta}; && \mathbf{r}^2 &=& (1, u-\sqrt{hg}, v)^T \\
\lambda^3 &=& \frac{u}{a\cos\theta}; && \mathbf{r}^3 &=& (0,0,1)^T
\end{array} \tag{13}$$

For a piecewise constant $\mathbf{q}$ the "jump" from two adjacent states Q_i and Q_{i-1} is defined as

$$\Delta\mathbf{q} = \begin{pmatrix} \Delta h' \\ \Delta(h'u) \\ \Delta(h'v) \end{pmatrix}. \tag{14}$$

where Δ is the difference operator $\Delta z = z_i - z_{i-1}$. The total contribution for all waves, $\mathcal{W}^k$, to the fluxes over cell interface $i - 1/2$ then becomes

$$\sum_{k=1}^{3} \tilde{\mathcal{W}}^k = \sum_{k=1}^{3} \tilde{\alpha}^k \tilde{\mathbf{r}}^k = \Delta\mathbf{q} \quad \Leftrightarrow \quad \left[\tilde{\mathbf{r}}^1, \tilde{\mathbf{r}}^2, \tilde{\mathbf{r}}^3\right] \begin{pmatrix} \tilde{\alpha}^1 \\ \tilde{\alpha}^2 \\ \tilde{\alpha}^3 \end{pmatrix} = \begin{pmatrix} \Delta h' \\ \Delta(h'u) \\ \Delta(h'v) \end{pmatrix}, \tag{15}$$

which gives

$$\tilde{\alpha}^1 = \frac{1}{2}\Delta h' + \frac{1}{2\sqrt{\tilde{h}g}}(\Delta(h'u) - \tilde{u}\Delta h') \tag{16}$$

$$\tilde{\alpha}^2 = \frac{1}{2}\Delta h' - \frac{1}{2\sqrt{\tilde{h}g}}(\Delta(h'u) - \tilde{u}\Delta h') \tag{17}$$

$$\tilde{\alpha}^3 = \Delta(h'v) - \tilde{v}\Delta h' \tag{18}$$

Here the ˜ indicates that a variable is evaluated at a cell interface.

The computed quantities, the state variables, Q_i, are cell centered average. To compute $\mathbf{A}$ and/or its eigenvalues/vectors at cell interfaces, we will have to find an approximation $\tilde{Q}$ based on the left state Q_{i-1} and the right state Q_i. In the nonlinear case $\tilde{Q} = Q_{i-1/2}$ can not be taken as a simple average between Q_i and Q_{i-1}. Roe [Roe81] established the following criteria for appropriate approximations:

1. It constitutes a linear mapping from the vector space $\mathbf{q}$ to the vector space $\mathbf{f}$.
2. As $Q_i \to Q_{i-1} \to \tilde{Q}, \quad \tilde{\mathbf{A}}(Q_i, Q_{i+1}) \to \mathbf{A}(\tilde{Q})$, where $\mathbf{A} = \partial\mathbf{f}/\partial\mathbf{q}$.
3. For any $Q_i, Q_{i-1}, \quad \tilde{\mathbf{A}}(Q_i, Q_{i-1}) \times (Q_i - Q_{i-1}) = F_i - F_{i-1}$.
4. The eigenvectors of $\tilde{\mathbf{A}}$ are linearly independent.

$\tilde{\mathbf{A}}\Delta Q = \Delta F$, based on (2) and (5), gives us the equations

$$\begin{aligned}
\frac{1}{a\cos\tilde{\theta}}\Delta(h'u) &= \Delta\left(\frac{h'u}{a\cos\theta}\right) && (19)\\
\frac{1}{a\cos\tilde{\theta}}\left(\left(-\tilde{u}^2 + \frac{\tilde{h}'g}{\cos\theta}\right)\Delta h' + 2\tilde{u}\Delta(h'u)\right) &= \Delta\left(\frac{h'u^2}{a\cos\theta} + \frac{h'^2 g}{2a\cos^2\theta}\right) && (20)\\
\frac{1}{a\cos\tilde{\theta}}(-\tilde{u}\tilde{v}\Delta h' + \tilde{v}\Delta(h'u) + \tilde{u}\Delta(h'v)) &= \Delta\left(\frac{h'uv}{a\cos\theta}\right) && (21)
\end{aligned}$$

In details the first equation becomes:

$$\frac{1}{\cos\theta_{i-1/2}}(h'_i u_i - h'_{i-1}u_{i-1}) = \frac{h'_i u_i}{\cos\theta_i} - \frac{h'_{i-1}u_{i-1}}{\cos\theta_{i-1}} \qquad (22)$$

which in general will NOT be satisfied. Note that the term which create problems is the $\cos\theta$ term. This is typical for non-autonomous equations. If we assume that $|\theta_i - \theta_{i-1}|$ is small, we expect $\cos\theta_i \approx \cos\theta_{i-1/2}$ and $\cos\theta_{i-1} \approx \cos\theta_{i-1/2}$. The equation then reduces to an identity and becomes redundant, giving us one degree of freedom for the three unknowns. They do however also have to satisfy property 2 above, $\tilde{h}' \to h'_i$ or h'_{i-1} when $h'_i \to h'_{i-1}$. A simple choice which satisfies this is

$$\tilde{h}' = \frac{1}{2}(h'_i + h'_{i-1}). \qquad (23)$$

Note that the error of (22) increases as $\theta_i \to \pm\pi/2$. Thus our approximations suffer from largest error closest to the poles.

Solving $\tilde{u}$ and $\tilde{v}$ from (20) and (21) using (23) gives

$$\begin{aligned}
\tilde{u} &= \frac{\sqrt{h'_i}u_i + \sqrt{h'_{i-1}}u_{i-1}}{\sqrt{h'_i} + \sqrt{h'_{i-1}}} && (24)\\
\tilde{v} &= \frac{\sqrt{h'_i}v_i + \sqrt{h'_{i-1}}v_{i-1}}{\sqrt{h'_i} + \sqrt{h'_{i-1}}} && (25)
\end{aligned}$$

After having found approximate values for the state variables at cell interfaces, we can decompose the fluxes into waves as shown in (15). The update to the cell average now consists of the contributions from right going waves at the left cell interface and from left going waves at the right cell interface. Thus (9) becomes:

$$Q_i^{n+1} = Q_i^n - \frac{\delta t}{\delta \phi}(\mathcal{A}^+ \Delta Q_{i-1/2} + \mathcal{A}^- \Delta Q_{i+1/2}) \tag{26}$$

where

$$\mathcal{A}^+ \Delta Q_{i-1/2} = \sum_{k=1}^{3} (\lambda_{i-1/2}^k)^+ \mathcal{W}_{i-1/2}^k; \quad \lambda^+ = \max(\lambda, 0) \tag{27}$$

and

$$\mathcal{A}^- \Delta Q_{i+1/2} = \sum_{k=1}^{3} (\lambda_{i+1/2}^k)^- \mathcal{W}_{i+1/2}^k; \quad \lambda^- = \min(\lambda, 0) \tag{28}$$

Inserting (27) and (28) into (26) gives

$$Q_i^{n+1} = Q_i^n - \frac{\delta t}{\delta \phi} \sum_{k=1}^{3} \left[\left(\lambda_{i-1/2}^k\right)^+ \mathcal{W}_{i-1/2}^k + \left(\lambda_{i+1/2}^k\right)^- \mathcal{W}_{i+1/2}^k \right]. \tag{29}$$

3.1.2 Wave decomposition in the θ direction

The eigendecomposition of $\mathbf{B}$ becomes

$$\begin{array}{rclrcl} \lambda^1 & = & \frac{v+\sqrt{hg}}{a}; & \mathbf{r}^1 & = & (1, u, v+\sqrt{hg})^T \\ \lambda^2 & = & \frac{v-\sqrt{hg}}{a}; & \mathbf{r}^2 & = & (1, u, v-\sqrt{hg})^T \\ \lambda^3 & = & \frac{v}{a}; & \mathbf{r}^3 & = & (0, 1, 0)^T \end{array} \tag{30}$$

$\tilde{\alpha}^k, \;\; k = 1, 2, 3$ is found to be

$$\tilde{\alpha}^1 = \frac{1}{2}\Delta h' + \frac{1}{2\sqrt{\tilde{h}g}}(\Delta(h'v) - \tilde{v}\Delta h') \tag{31}$$

$$\tilde{\alpha}^2 = \frac{1}{2}\Delta h' - \frac{1}{2\sqrt{\tilde{h}g}}(\Delta(h'v) - \tilde{v}\Delta h') \tag{32}$$

$$\tilde{\alpha}^3 = \Delta(h'u) - \tilde{u}\Delta h' \tag{33}$$

Solving the equations given by $\tilde{\mathbf{B}}\Delta Q = \Delta G$, corresponding to (19, 20 and 21), provides the same approximated values for $\tilde{h}$, $\tilde{u}$ and $\tilde{v}$ as in the ϕ-direction.

3.1.3 Second order correction

The wave-propagation method (26) can be extended to a second order method by adding correction terms to the flux update,

$$Q_i^{n+1} = Q_i^n - \frac{\delta t}{\delta\phi}\left(\mathcal{A}^+\Delta Q_{i-1/2} + \mathcal{A}^-\Delta Q_{i+1/2}\right) - \frac{\delta t}{\delta\phi}\left(\hat{F}_{i+1/2} - \hat{F}_{i-1/2}\right) \quad (34)$$

where

$$\hat{F}_{i\pm1/2} = \frac{1}{2}\sum_{k=1}^{3}|\lambda_{i\pm1/2}^k|\left(1 - \frac{\delta t}{\delta\phi}|\lambda_{i\pm1/2}^k|\right)\hat{\mathcal{W}}_{i\pm1/2}^k. \quad (35)$$

Here $\hat{\mathcal{W}}_{i\pm1/2}^k$ represents a limited version of the waves $\mathcal{W}_{i\pm1/2}^k$. $\hat{\mathcal{W}}_{i-1/2}^k$ is obtained by comparing $\mathcal{W}_{i-1/2}^k$ to $\mathcal{W}_{i-3/2}^k$ if $\lambda_{i-1/2}^k > 0$ or $\mathcal{W}_{i+1/2}^k$ if $\lambda_{i-1/2}^k < 0$.

The purpose of a limiter is to counter the dispersive nature of a high-resolution method. A limiter can also remove phase errors. CLAWPACK provides several different limiters, and in this work the monotonized centered (MC) limiter [vL77] have been chosen.

3.2 Flux-based wave-propagation algorithm

Lately a new method for decomposing the waves has been suggested [BLMR03]. The idea is to work with the fluxes directly rather than decomposing the Jacobian of the quasi-linear advection form.

The flux difference $\Delta\mathbf{f}$ (in the ϕ-direction) is directly decomposed as a linear combination of the eigenvectors of $\tilde{\mathbf{A}}$:

$$\Delta\mathbf{f} = \sum_{k=1}^{3}\tilde{\beta}^k\tilde{\mathbf{r}}^k = \sum_{k=1}^{3}\tilde{\mathcal{Z}}^k \quad \Leftrightarrow \quad [\tilde{\mathbf{r}}^1, \tilde{\mathbf{r}}^2, \tilde{\mathbf{r}}^3]\begin{pmatrix}\tilde{\beta}^1\\ \tilde{\beta}^2\\ \tilde{\beta}^3\end{pmatrix} = \begin{pmatrix}\Delta\left(\frac{h'u}{a\cos\theta}\right)\\ \Delta\left(\frac{h'u^2}{a\cos\theta} + \frac{h'^2 g}{2a\cos^2\theta}\right)\\ \Delta\left(\frac{h'uv}{a\cos\theta}\right)\end{pmatrix}. \quad (36)$$

The vectors $\tilde{\mathcal{Z}}^k = \tilde{\beta}^k\mathbf{r}^k$ is called *f-waves*, as they are analogue to the waves $\tilde{\mathcal{W}}^k$, but carry flux increments rather than increments in $\mathbf{q}$. When solving (36) for β_1, β_2 and β_3 we approximate $\tilde{\mathbf{r}}^k$ with the values from (23, 24 and 25). (9) can now be replaced by

$$Q_i^{n+1} = Q_i^n - \frac{\delta t}{\delta\phi}\left[\sum_{\forall k:\, \lambda_{i-1/2}^k>0}\mathcal{Z}_{i-1/2}^k + \sum_{\forall k:\, \lambda_{i+1/2}^k<0}\mathcal{Z}_{i+1/2}^k\right]. \quad (37)$$

An advantage of using (36) instead of (15), is that the f-waves method is conservative even if the third of Roe's criteria is not satisfied. This was exactly what caused trouble when we were trying to construct our Roe average values.

Note that in the case where the standard wave decomposition does satisfy property 3, $\tilde{\beta}^k = \tilde{\alpha}^k\tilde{\lambda}^k$ and hence $\tilde{\mathcal{Z}}^k = \tilde{\lambda}^k\tilde{\mathcal{W}}^k$ and the two methods become equivalent.

As for the standard method of (26), f-waves method can be extended to a second order method by adding correction terms. In this case the correction term of (29) takes the following form:

$$\hat{F}_{i\pm1/2} = \frac{1}{2}\sum_{k=1}^{3} \operatorname{sgn}\left(\lambda^k_{i\pm1/2}\right)\left(1 - \frac{\delta t}{\delta\phi}|\lambda^k_{i\pm1/2}|\right)\hat{\mathcal{Z}}^k_{i\pm1/2} \tag{38}$$

Here $\hat{\mathcal{Z}}^k_{i\pm i/2}$ is a limited version of the f-wave $\mathcal{Z}^k_{i\pm1/2}$ obtained in the same manner as $\hat{\mathcal{W}}^k_{i\pm1/2}$ would be obtained.

3.3 Entropy fix

The wave-propagation scheme used above splits the waves in left going and right going. For constant initial value each wave propagates with constant speed. In the non-linear case and piecewise constant initial values the speeds of waves form neighboring cells have usually different speed, causing shocks or rarefaction waves. This does however usually not cause any problems for estimating fluxes over cell boundaries as long as the time-step is bounded by the CFL-criterion. The exception being for transonic rarefaction waves. This occurs whenever $\lambda^k_{i-1} < 0 < \lambda^k_i$. In these cases care must be taken and an entropy fix should be implemented.

We have adopted the standard CLAWPACK technique and implemented the procedure proposed by Harten and Hyman [HH83]. Here a fraction of the wave, γ, is supposed to be left going, while $1-\gamma$ is said to be right going. This allows for a simple modification of the code.

3.4 The source term

3.4.1 Operator splitting

Like the dimension splitting the source term splitting in (7) and (8) introduces errors. To solve the combined system we are using the second order

Strang splitting ([Str68]). When the splitting error is of the same order as the numerical discretization error, it is usually regarded as acceptable, but may in some cases lead to unphysical solutions. In particular this might happen in the case of a stationary flow. For $\mathbf{q}_t$ to stay zero, one actually rely on two errors to cancel each other.

To solve (8) we have implemented a low order explicit Runge-Kutta method.

3.4.2 Handling balance laws using f-waves

Irregular topography in SWE is modeled by adding $-ghB_\phi$ in the second equation of the right hand side (3) and $-ghB_\theta$ of the third, respectively. $B(\phi, \theta)$ is the bottom elevation. Source terms like these, with a well defined spatial direction can be incorporated in the f-waves. This is done by evaluating the source term $\tilde{\mathbf{s}}$ at the cell interfaces, and then computing f-waves, $\tilde{\mathcal{Z}}^k$, as a decomposition of

$$\Delta \mathbf{f} - (\delta\phi)\tilde{\mathbf{s}} = \sum_{k=1}^{3} \tilde{\beta}^k \tilde{\mathbf{r}}^k = \sum_{k=1}^{3} \tilde{\mathcal{Z}}^k \tag{39}$$

and analogously in the other spatial direction.

This approach to handling source terms is useful particular in cases where the solution is close to a steady state in which the flux gradient should nearly balance the source term.

Source term $\mathbf{s}$ of (3) does not lend itself to this kind of decomposition as it has terms which mixes the spatial dimensions.

4 The computational grid

A sketch of a physical grid covering the sphere and the computational grid representing the physical grid is shown in Figure 1. A physical sphere is of course unbounded or equivalently periodic. The computational, rectangular (ϕ, θ) grid also becomes periodic in the ϕ-direction, but problems occurs in the θ-direction at poles. The singularities apparent in the equations for $\theta = \pm\pi/2$ is reflected in the geometrical transformation of a spherical triangle into a rectangle. Whenever we would like to compute fluxes over the (computational) cell interface corresponding to a pole-point we are faced with the singularity of the equations. However, it is reasonably to argue that since

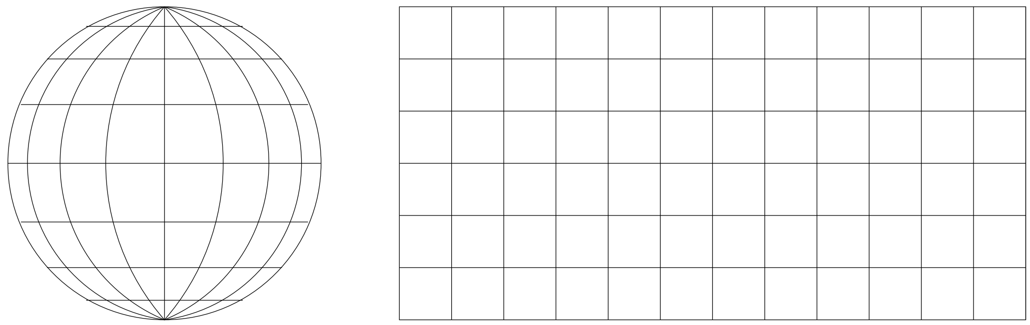

Figure 1: *The physical and the computational grid*

this cell interface degenerate to zero-size no physical masses or velocities can be transported across this interface and consequently we have set the fluxes to zero at the "pole"-interfaces. Figure 2 shows the correspondence between a physical cell at the North pole and the computational cell.

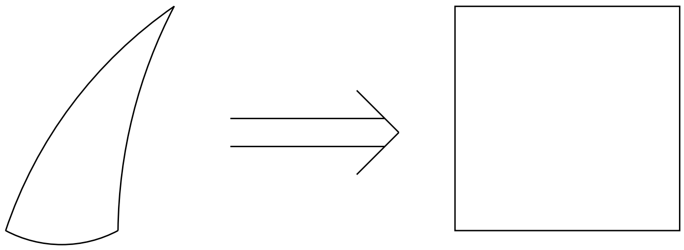

Figure 2: *The correspondence between a physical cell at the North pole and the computational cell*

Note that only flux-computation is subject to "zero-division" as Q_{ij}^n is computed at cell-center and the cell center closest to the pole is at $\pm(\pi/2 - \Delta\theta/2)$, where $\Delta\theta$ is the cell size.

5 Experiments

In this section we report experimental results from applying the methods outlined in the previous sections to test cases from the standard test suite for the spherical SWE by Williamson et al. [WDH$^+$91].

The following constants have been used in the computation:

$$\Omega = 7.292 \cdot 10^{-5} s^{-1} \tag{40}$$

$$a = 6.37122 \cdot 10^{6} m \ (The\ earth'\ radius) \tag{41}$$

$$g = 9.80616 m/s^2 \tag{42}$$

Error measures

It is in the description of the test problems [WDH+91] also specified how to report the results. They should be documented by surface maps of h and the error in h after five days. In addition, graphs of the L_1, L_2 and L_∞ errors of h and the velocities u, v versus time should be included. The precise definitions of these error measures are:

Define I to be a discrete approximation to the global integral

$$I[h] = \frac{1}{4\pi} \int_0^{2\pi} \int_{-\pi/2}^{\pi/2} h(\phi, \theta) \cos\theta \, d\theta \, d\phi. \tag{43}$$

If the true (and initial) solution is given by h_T, u_T and v_T, the normalized global errors of h are given by

$$L_1(h) = \frac{I[|h(\phi,\theta) - h_T(\phi,\theta)|]}{I[|h_T(\phi,\theta)|]} \tag{44}$$

$$L_2(h) = \frac{\{I[(h(\phi,\theta) - h_T(\phi,\theta))^2]\}^{\frac{1}{2}}}{\{I[h_T(\phi,\theta)^2]\}^{\frac{1}{2}}} \tag{45}$$

$$L_\infty(h) = \frac{\max_{\forall\phi,\theta} |h(\phi,\theta) - h_T(\phi,\theta)|}{\max_{\forall\phi,\theta} |h_T(\phi,\theta)|} \tag{46}$$

and the normalized global errors of the velocities u, v by

$$L_1(u,v) = \frac{I\left[\{(u(\phi,\theta) - u_T(\phi,\theta))^2 + (v(\phi,\theta) - v_T(\phi,\theta))^2\}^{\frac{1}{2}}\right]}{I\left[\{u_T(\phi,\theta)^2 + v_T(\phi,\theta)^2\}^{\frac{1}{2}}\right]} \tag{47}$$

$$L_2(u,v) = \frac{\{I\left[(u(\phi,\theta) - u_T(\phi,\theta))^2 + (v(\phi,\theta) - v_T(\phi,\theta))^2\right]\}^{\frac{1}{2}}}{\{I\left[u_T(\phi,\theta)^2 + v_T(\phi,\theta)^2\right]\}^{\frac{1}{2}}} \tag{48}$$

$$L_\infty(u,v) = \frac{\max_{\forall\phi,\theta}\left[\{(u(\phi,\theta) - u_T(\phi,\theta))^2 + (v(\phi,\theta) - v_T(\phi,\theta))^2\}^{\frac{1}{2}}\right]}{\max_{\forall\phi,\theta}\left[\{u_T(\phi,\theta)^2 + v_T(\phi,\theta)^2\}^{\frac{1}{2}}\right]}. \tag{49}$$

5.1 Test case 2: Global steady state nonlinear zonal geostrophic flow

This case is a steady state solution to the non-linear SWE outlined in Section 2. It consists of solid body rotation of a zonal geostrophic flow.

The angle between the axis of the solid body rotation and the polar axis of the spherical coordinate system is denoted by α (not to be confused with $\tilde{\alpha}$ in Section 3), so that several orientations can be specified.

The velocity fields are initially (and for all time)

$$\begin{aligned} u &= u_0(\cos\theta\cos\alpha + \cos\phi\sin\theta\sin\alpha) && (50) \\ v &= -u_0\sin\phi\sin\alpha && (51) \end{aligned}$$

while the analytic h field is given by

$$gh = gh_0 - (a\Omega u_0 + \frac{u^2}{2})(-\cos\phi\cos\theta\sin\alpha + \sin\theta\cos\alpha)^2 \qquad (52)$$

and the Coriolis parameter by

$$f = 2\Omega(-\cos\phi\cos\theta\sin\alpha + \sin\theta\cos\alpha). \qquad (53)$$

Here

$$\begin{aligned} u_0 &= \frac{5^5 m}{3^4 s} \approx 38.58ms^{-1} && (54) \\ gh_0 &= 29400m^2s^{-2}. && (55) \end{aligned}$$

The tests should be done for $\alpha = 0.0, 0.05, \pi/2$ and $\pi/2 - 0.05$.

Note that the denominator in (49) is zero for $\sin\phi = 0$ and $\tan\theta = -1/\tan\alpha$. For discrete values of (ϕ, θ), we can hope to avoid the zeroes, but very small values of the denominator is doomed to appear. These will of course magnify any minor absolute error, making this error measure meaningless for this test case.

Note also that the given values for u_0 and gh_0 imply that $\sqrt{gh} > 96$ and $u < 2u_0 = 77.16$. Consequently the sign of a specific eigenvalue given in (13) is the same on both side of a cell interface and thus the entropy fix will never be executed.

All our tests are done on a 100×100 grid with $\phi \in [-\pi, \pi]$ and $\theta \in [-\pi/2, \pi/2]$, using the methods described in Section 3. In all test runs conservation of mass were obtained.

5.1.1 Numerical results for $\alpha = 0.0$

The initial state for $\alpha = 0.0$ is shown in Figure 3.

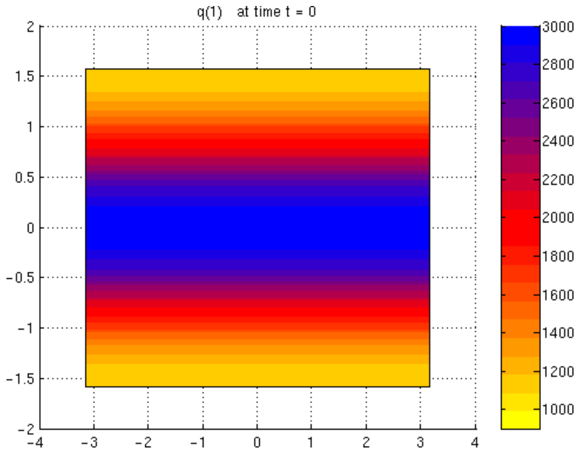

Figure 3: *Test case 2,* $\alpha = 0.0$*. The initial configuration.*

Standard wave-propagation method

First we tested the standard wave-propagation method, using first and second order wave approximation.

For the first order method, shown in Figure 4, the final state (after five days) shows huge deviations from the original state, as can also be seen in the error difference plot of h. The fluid has been reduced at equator, causing a build-up at physical small cells near the pole. The depth at the poles has increased to 9000m after five days!

Great improvements are seen when introducing the second order method as shown in Figure 5, but the same pattern is still seen. The error is great near the poles. The error in cells closest to the pole dictates the $L_\infty(h)$ norm and makes this unacceptable high. Another disturbing feature is the oscillating nature of the solution. This should not happen to a steady state solution. The magnitude of the error does however not increase after an initial blow up, but stays within a fixed band.

As these results shows, the standard wave propagation method is not a good way of solving our problem. One reason for this is that (22) is not satisfied, and consequently the averaging procedure of (23, 24 and 25) used in our code does not satisfy Roe's criteria.

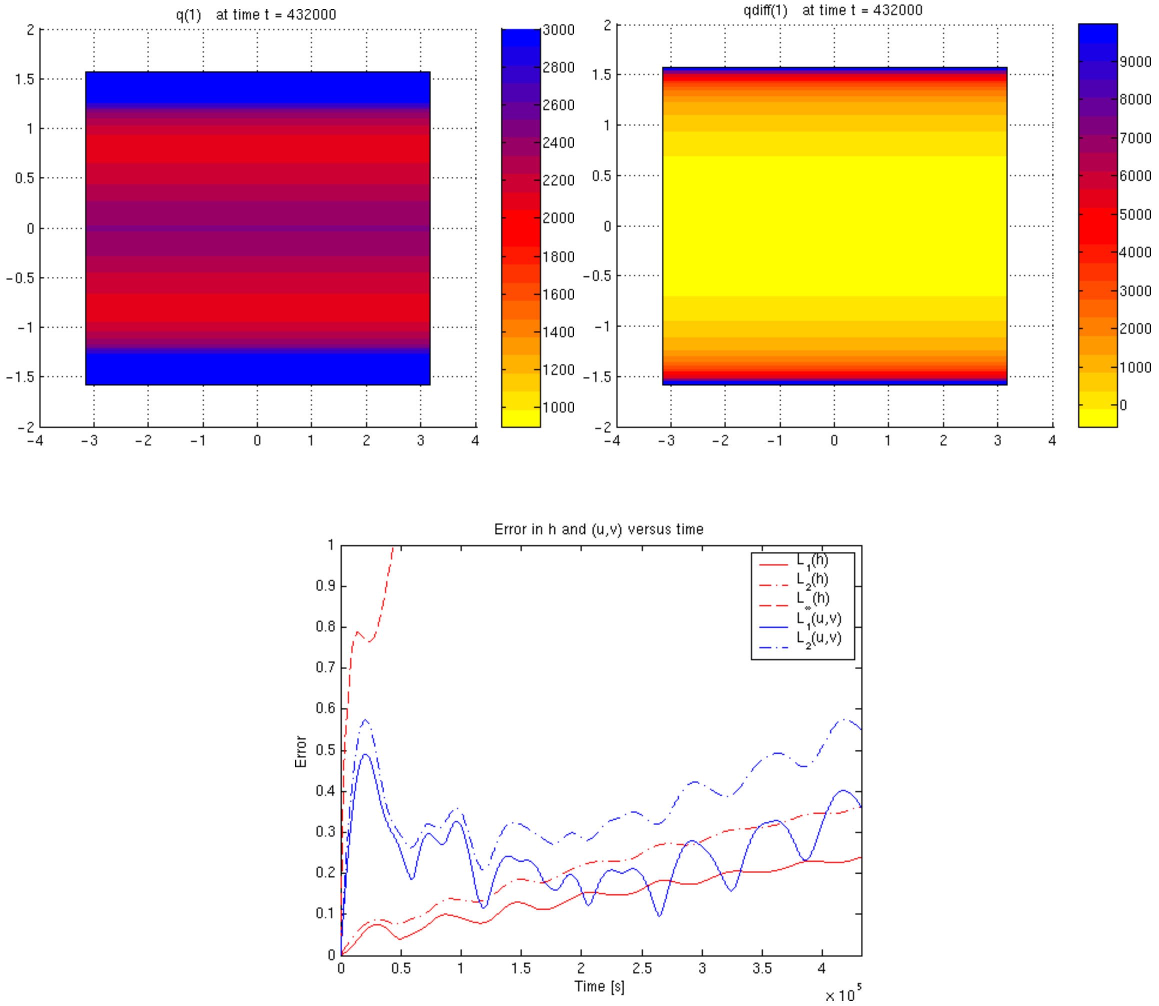

Figure 4: *Test case 2, $\alpha = 0.0$. Standard wave-propagation method. 1st order Godunov's method, 1st order source term solver. Upper left: State at $T = 432000s = 5$ days, Upper right: Plot of error difference in h after 5 days, Lower: Graphs of normalized errors of h and u, v.*

Flux-based wave-propagation method

For the flux-based wave-propagation method the Roe criteria is not required anymore. By circumventing one of the problems observed we hoped for improvement with this method and undertook the same set experiment as for the standard waves method.

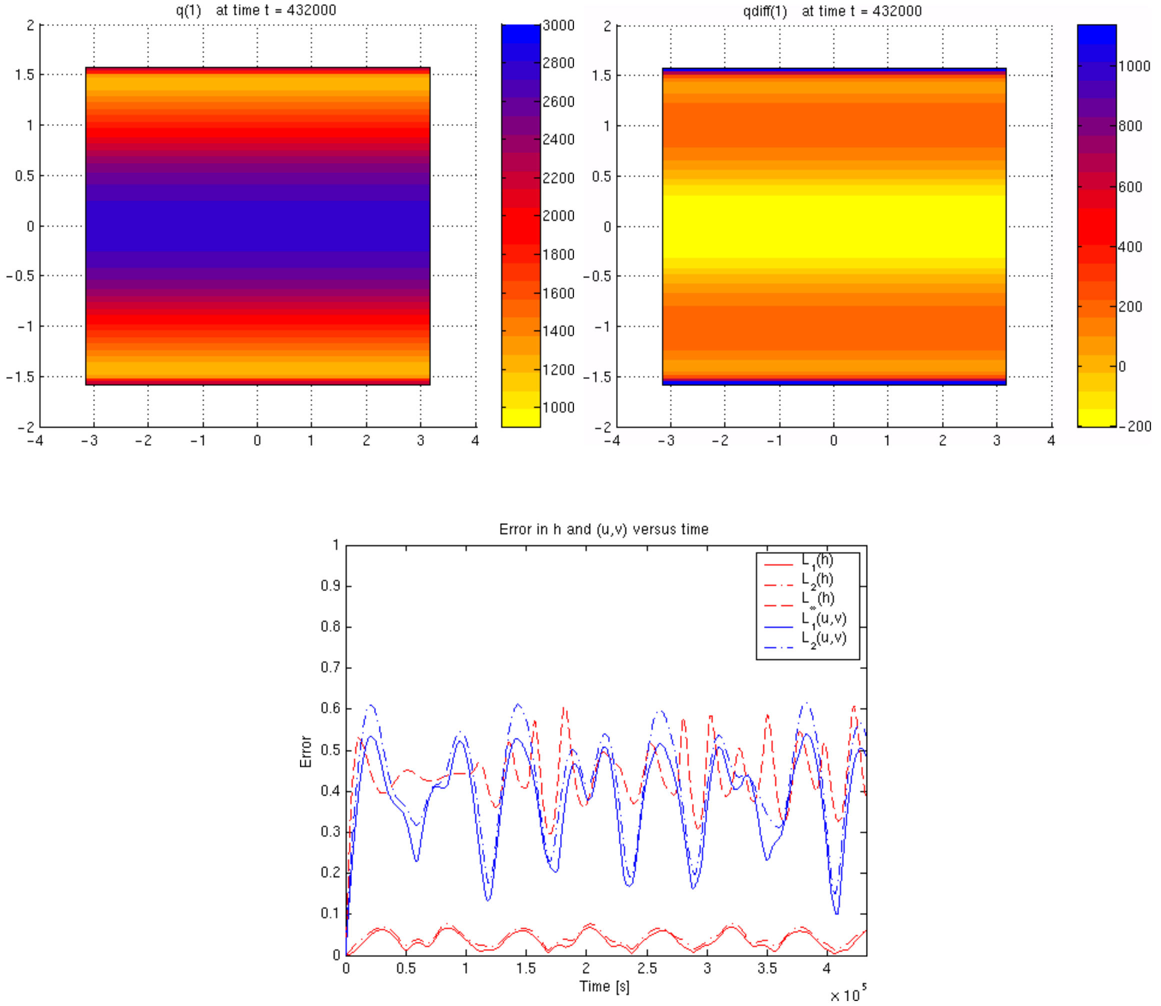

Figure 5: *Test case 2,* $\alpha = 0.0$*. Standard wave-propagation method. Godunov's method with 2nd order correction, 2nd order source term solver. Upper left: State at* $T = 432000s = 5$ *days, Upper right: Plot of error difference in* h *after 5 days, Lower: Graphs of normalized errors of* h *and* u, v*.*

For the first order method, shown in Figure 6, the five day simulation is still far from the correct results, and the error increases in time. The increased depth at the poles is still present, but not as large as for the standard wave-propagation method.

In Figure 7 we have added second order correction to the scheme. As

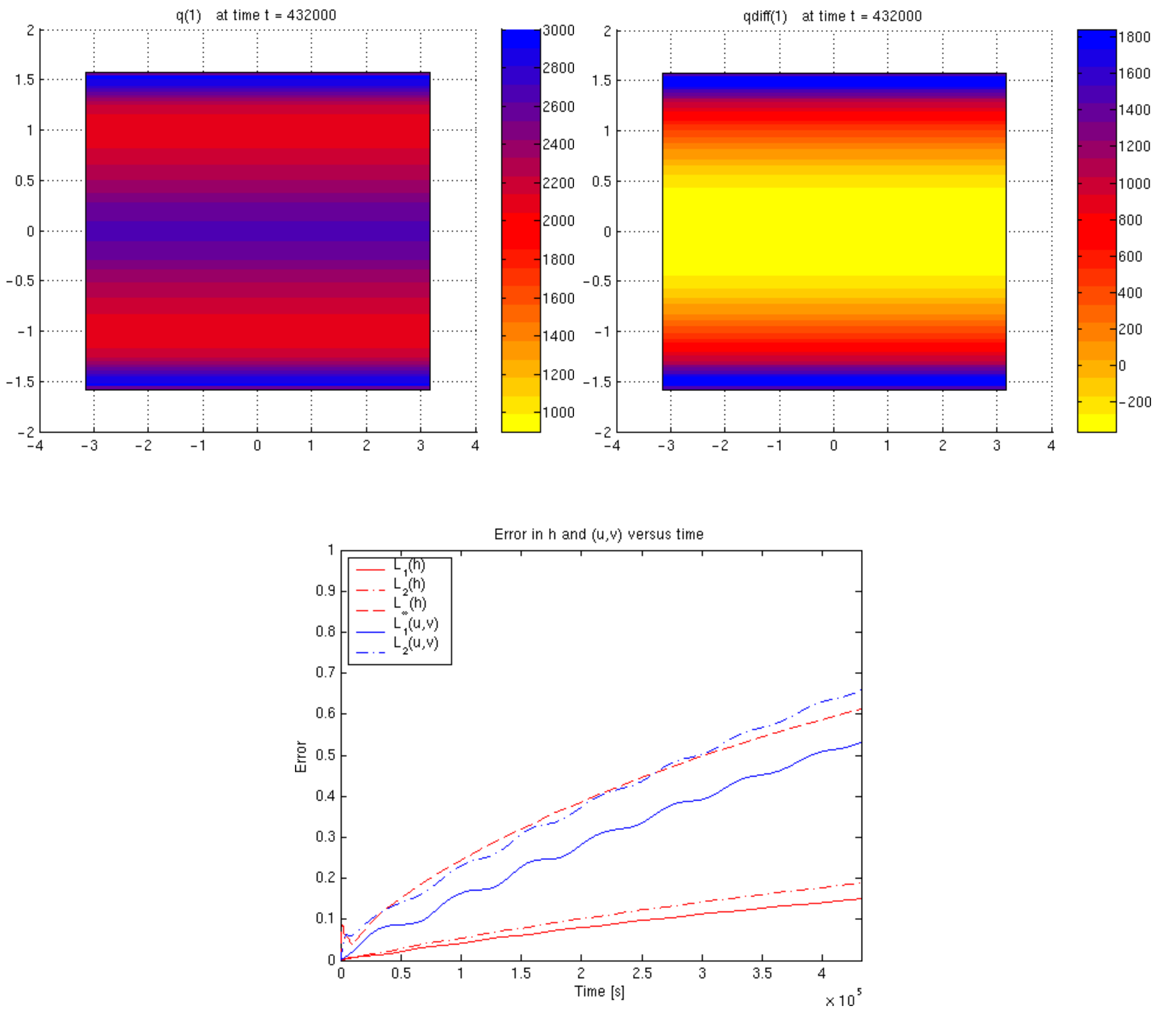

Figure 6: *Test case 2,* $\alpha = 0.0$*. Flux-based wave-propagation method. 1st order Godunov's method, 1st order source term solver. Upper left: State at* $T = 432000s = 5$ *days, Upper right: Plot of error difference in* h *after 5 days, Lower: Graphs of normalized errors of* h *and* u, v*.*

is evident from these figures the second order scheme greatly improves the accuracy of the computation. But as the error-plot shows, there is still a major problem near the poles. This time the built-up of mass near the poles have been replaced by a sink. We also notice from the plot of error-norms that the overall error-norms is still increasing with time. Thus no steady

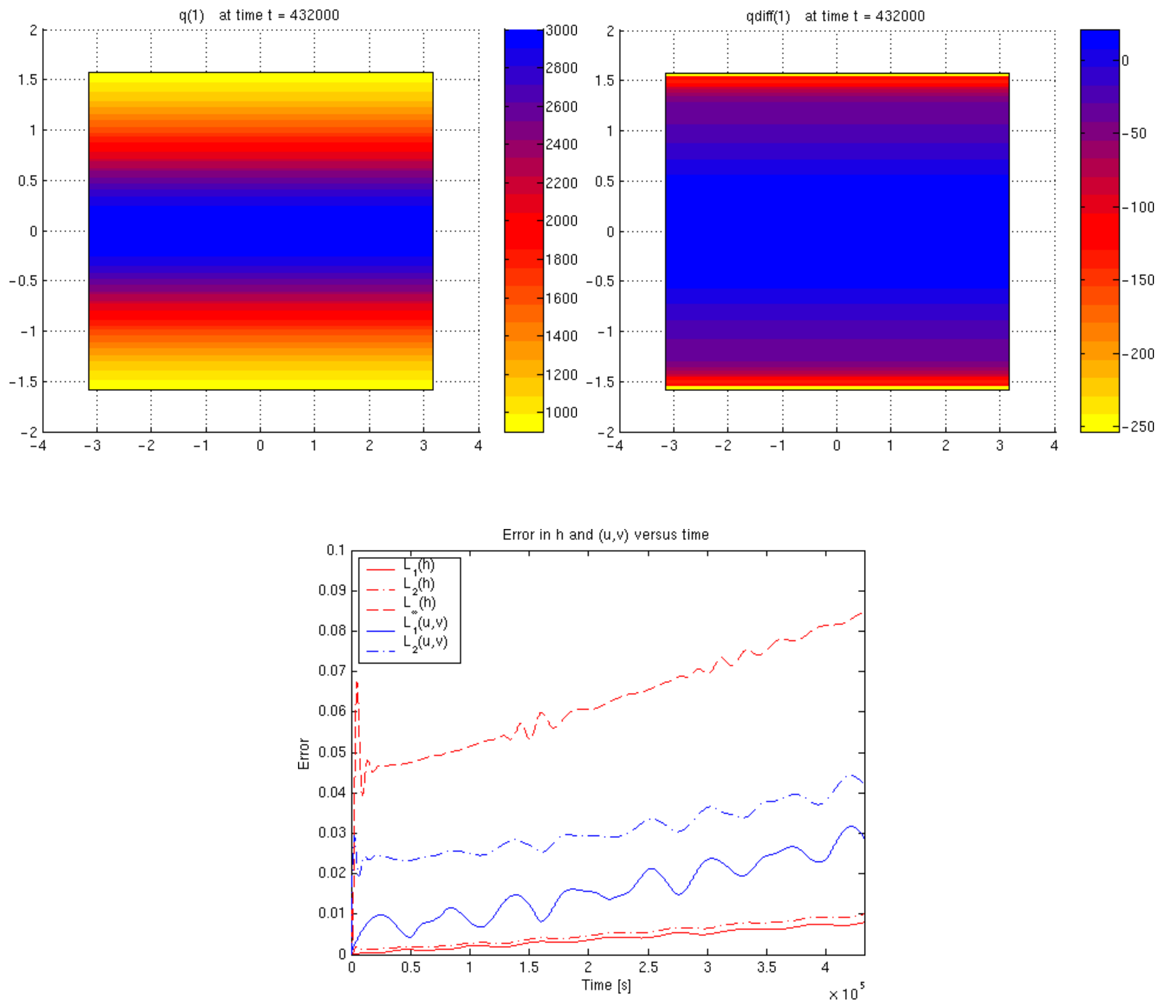

Figure 7: *Test case 2, $\alpha = 0.0$. Flux-based wave-propagation method. Godunov's method with 2nd order correction, 1st order source term solver. Upper left: State at $T = 432000s = 5$ days, Upper right: Plot of error difference in h after 5 days, Lower: Graphs of normalized errors of h and u, v.*

state has been reached. (Note that the unit of the errors has been reduced with a factor 10 from Figure 6 to Figure 7.)

The final improvement made is to also solve the source term with a second order method. Now the computed solution becomes very close to the true solution with exception of the cells close to the poles. Even more pleasing is the fact that the error quickly reaches a constant level. This is shown in

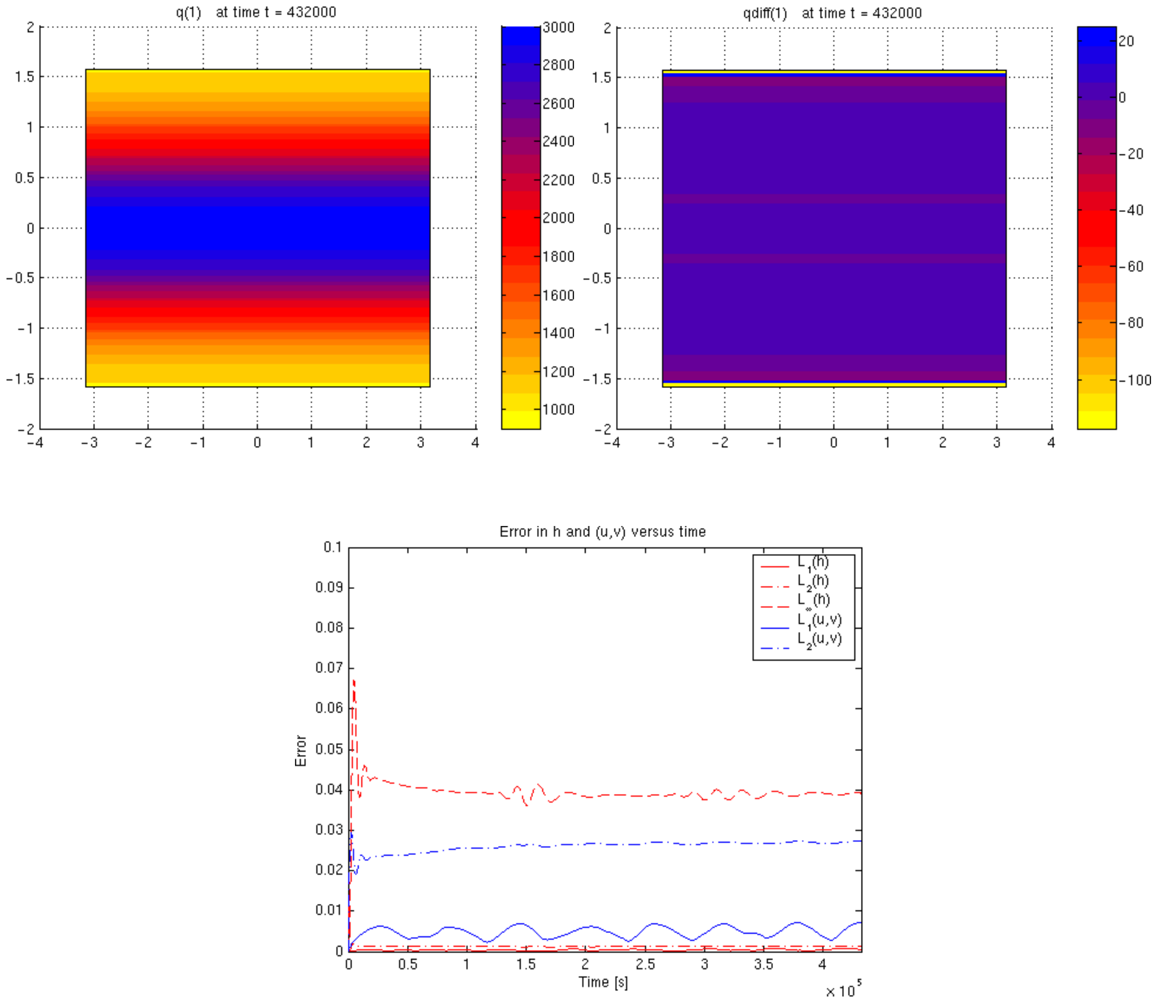

Figure 8: *Test case 2, $\alpha = 0.0$. Flux-based wave-propagation method. Godunov's method with 2nd order correction, 2nd order source term solver. Upper left: State at $T = 432000s = 5$ days, Upper right: Plot of error difference in h after 5 days, Lower: Graphs of normalized errors of h and u, v.*

Figure 8. Apparently it has converged to a steady state, very close to the initial state.

That we do not get exactly the same state as initially, should not come as any surprise. Using the split operator technique we are not anymore solving the exact system, but a slightly perturbed problem. The f-waves method appears to find a stable steady state solution for this perturbed problem.

After some initial oscillation it quickly finds a steady state, close to the true solution. The standard waves, however, produce an unstable solution oscillating around the perturbed solution.

As the error-plots convincingly show, the main errors occurs near the poles. This is also the reason why $L_\infty(h)$ consistently is so much larger then the other two error measures for h.

We are convinced that the pole-problem we observe is a consequence of spherical coordinates and the computational grid we are applying. The minor perturbation of the problem near equator propagates toward the poles. Here there is no escape, and as conservation is required, a few physically small cells have to compensate for the minor displacements of mass, producing relatively large errors in these cells. No such problem is observed in the east-west direction. Here the implementation of periodic boundary conditions correctly mimics the physic.

5.1.2 Numerical results for $\alpha = \pi/2$

With the axis of the rotating zonal flow orthogonal to the axis of the sphere we have a strong flow component in the latitude direction. This flow direction is expected to create severe problems for our technique for handling boundaries in the latitude direction.

The initial state for $\alpha = \pi/2$ is shown in Figure 9.

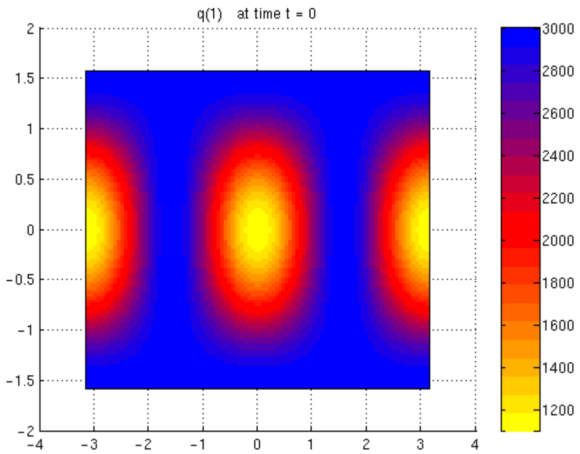

Figure 9: *Test case 2, $\alpha = \pi/2$. The initial configuration.*

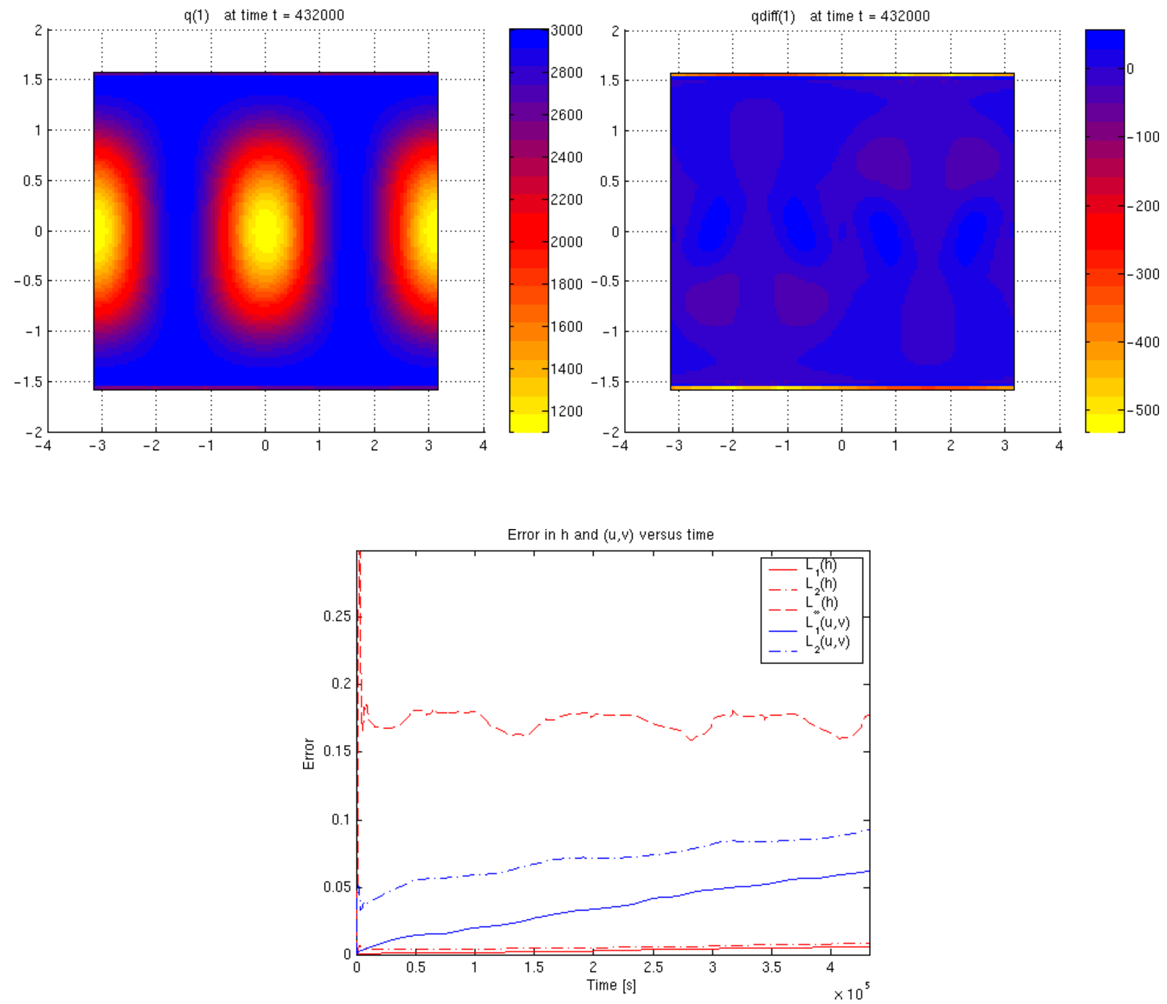

Figure 10: *Test case 2,* $\alpha = \frac{\pi}{2}$*. Flux-based wave-propagation method. Godunov's method with 2nd order correction, 2nd order source term solver. Upper left: State at* $T = 432000s = 5$ *days, Upper right: Plot of error difference in* h *after 5 days, Lower: Graphs of normalized errors of* h *and* u, v*.*

Flux-based wave-propagation, second order

The results here are shown in Figure 10. The errors are overall larger, but shows a surprisingly familiar pattern: relative small error at equator, larger error in pole regions. The error-norm for h is stable, but now we observe a small increase in the error of the fluxes.

This gives evidence to our hypothesis that the problem we see is related to the discretization grid we use. The unphysical handling of boundaries becomes a larger problem with a strong flow crossing the poles.

5.1.3 Other values of α

We have run similar tests for $\alpha = 0.05$ and $\alpha = \pi/2 - 0.05$. The results are not presented here as they gave no new insight. The case for $\alpha = 0.05$ behaved almost identical to the case $\alpha = 0.0$, while the case $\alpha = \pi/2 - 0.05$ behaved as $\alpha = \pi/2$.

5.1.4 Rate of convergence

In addition to measuring error-norms, [WDH+91] require that the $L_2(h)$ and $L_\infty(u, v)$ errors at five days should be used to measure the rate of convergence for the method. Since all the choices of α seemed to give comparable results for the same method, we have chosen to only study the rate of convergence for $\alpha = 0.0$ and second order flux-based wave-propagation method. The results are presented in Table 1.

Resolution	$L_1(h)$	CR	$L_2(h)$	CR	$L_\infty(h)$	CR
50×50	0.0031		0.0044		0.0412	
100×100	0.0005	5.6	0.0013	3.3	0.0392	1.1
200×200	0.0001	5.2	0.0006	2.1	0.0439	0.9

Resolution	$L_1(u, v)$	CR	$L_2(u, v)$	CR
50×50	0.0216		0.0603	
100×100	0.0070	3.1	0.0272	2.2
200×200	0.0017	3.9	0.0119	2.3

Table 1: *Errors after 5 days and corresponding convergence rates (CR) compared to the one step coarser grids errors.*

Measured by $L_\infty(h)$ there is no sign of convergence. This measurement is dictated by cells close to the poles and highlight the well known and clearly observed pole-problem produced by our discretization of the sphere. All the other error measurements show clear evidence of quadratic convergence. If the pole-cells is omitted when computing $L_\infty(h)$ the quadratic convergence for a second order scheme is observed here too.

5.2 Test case 3: Steady state nonlinear zonal geostrophic flow with compact support

As in Test case 2, this test case is also a zonal flow. However, here the longitude velocity, u, is zero outside a band. As for Test case 2 the rotation body may have an angle, α, with the polar coordinate system. For $\alpha = 0$ we have zero velocities at the poles. We might hoped that this fact would eliminate the pole-problem. But that turned out not to be the case. We saw exactly the same behavior as for Test case 2. A small, almost neglectable error near the equator propagated rapidly toward the poles. Here these small perturbation were accumulated on very small physical cells, causing relative large errors in these.

6 Discussion

6.1 Alternative discretization strategies

Since its introduction in 1970 [Orz70, EMR70] various version of the spectral transform method (STM) [Swa00, Gat92] have been the main vehicle for solving global circulation problems. The STM is approximating the equation on a regular latitude-longitude grid. These grids usually present a number of problems at or near the poles, which can be elegantly handled for STM methods using a filtering technique. Lately some concerns have been raised on the efficiency of STM methods on next generation high performance computers. The same global interactions which gives the spectral methods its high accuracy, has proved to impose high communication costs with respect to parallelization. Also in cases where local refinement is called for, spectral methods are hard to apply, as they are designed for a fixed global grid.

For that reason there has been a renewed interest in discretization schemes which only involves local computation. Finite element schemes (FEM), first introduced into hydrodynamics in 1973 [Gro73], have lately attracted a lot of interest (See [Beh98, Hei02, CS90, CDMW98a, CDMW98b, DM00] and references therein. Using only local information for updating, explicit FEM methods usually have an easy and scalable parallel version. Combined with semi-Lagrangian time stepping high efficiency is also possible to achieve. As FEM does not rely on a regular grid there is no need to stick to the latitude-longitude grid anymore. Any grid of spherical triangles or rectangles will do and might be combined with a refinement strategy. On such a grid the poles do not need any special treatment. A main problem for these methods appears to be obtaining conservation.

Spectral element methods [TTI97] can be viewed as an attempt to combine the flexibility of the FEM with the high accuracy of the STM.

FEM's problem with conservation serves as a motivation for trying finite volume methods (FVM). By its very design criterion these technique guaranty conservation. At the same time they share the local property of FEM methods. In principal they are not restricted to regular grids, but in practice most implementation are based on a regular discretization.

6.2 Problems with FVM and how to deal with them

The only reason why there are so many alternative methods for the problem at hand is that no method is superior with respect to all possible measures like accuracy, efficiency, reliability, conservation, flexibility, scalable parallel version, etc... In this subsection we highlight problems with our method and suggest improvements. In our implementation we met two major obstacles. The first one is related to solving steady state problems. Of course one may argue that this is an artificial problem for a code designed for dynamic problems, but nevertheless we feel it is fair to require that the method solves such problems satisfactory because one might happen to stumble a cross such a problem unknowingly and because we are fundamental skeptical to a claim that a method not solving a "simple" problem (steady state), is able to solve more difficult problems (dynamic problems).

The clue to successfully dealing with steady state problems (or near steady state) appears to be the new flux-based wave-propagation scheme [BLMR03] combined with second order accurate scheme. In all test cases this gave us a steady state solution. That the steady state is not exactly the one prescribed is due to the splitting error introduced by the split-operator technique applied. In 2-norm and 1-norm the global error is not unacceptable high, but the distribution of the error, with huge error in cells close to the poles, revealed the second major problem related to the computational grid.

Implementing this problem with a reasonable effort was made possible using CLAWPACK [LLBM00]. CLAWPACK is based on using a rectangular computational grid. We constructed our by the standard mapping of longitude and latitude to a Cartesian grid. This gave a number of problems. While the regularity of the sphere is possible to maintain by using periodic boundary conditions in the longitude direction this is not easily obtained in the latitude direction. Physically the cell interfaces at the pole-point has zero extension, thus one can argue that no flow should pass through this interface. However, as the splitting technique causes a small perturbation in the solution we saw some minor propagation of mass. The pole-cells, where there was no escape, had to pay for this, as the total mass had to be conserved. Being of small physical size, the small shift of mass to or from these cells made a huge impact on the hight level in these cells.

Our grid also led to computational inefficiency as it gave very short time steps. The time steps are dictated by the need to obey the CFL-criterion. This is simply

$$\max_{i,j,m}(\lambda^m_{i,j})\delta t/\delta\phi < 1. \tag{56}$$

For fixed $\delta\phi$ and $\delta\theta$ and relative uniform h and u, the eigenvalues of (13) is dictated by $\cos\theta$. Appearing in the denominator this term is blowing up the eigenvalues near $\theta = \pm\pi/2$ and through the CFL-criterion forcing the time step down.

6.3 Mesh refinement

Observing that the computational problem is located to a small area, one might be tempted to try reducing the error by local grid refinement. This is easy using CLAWPACK as associated with CLAWPACK is M. Berger et al.'s successful adaptive mesh refinement (AMR) algorithm [BO84, BC84], combined with CLAWPACK in the package AMRCLAW [BL97, BL98]. We tried AMRCLAW on our pole-problem, but found that grid refinement is not the right answer to it. The reason is that the problem is artificial in the sense that the huge gradients and errors in h, seen near the poles is not caused by physics, and consequently the errors observed is not a result of fine scale phenomena which only can be resolved on a finer grid. The problem is related to a fundamental flaw in the computational grid, to which grid refinement is not the answer. This phenomena is illustrated by $L_\infty(h)$ in Table 1. No improvement is seen as we refine the cells.

In fact new problems occurred when trying AMRCLAW. For cells refined R times AMRCLAW also refines the time step R times. Assuming the eigenvalues on refined cells is approximately the same as for large cell this is the right thing to do in order to fulfill the CFL-criterion. However, with grid cells of size $\delta\theta$ the eigenvalues of pole-cells has a factor $1/cos(\pi/2 - \delta\theta/2) \approx 2/\delta\theta$. When refined this factor becomes $2R/\delta\theta$. Implying that we need to refine the time step with a factor R^2 to still be in compliance with the CFL-criterion.

6.4 Alternative grids

A better computational grid is probably achieved by first splitting the sphere into congruent regular spherical polygon and then refine these pieces. There do exist only five Platonic solids which do this [Alf97]. Three are based on triangles, the tetrahedron, the octahedron and the icosahedron. One is the dodecahedron which are based on regular pentagons. The last one is the hexahedron which is based on squares. This is the natural choice to be used with CLAWPACK, as its unit cell is a rectangle. A mapping of the spherical cube is illustrated in Figure 11. As indicated in the figure, each of the faces should be mapped to a square and the the boundaries of each such square

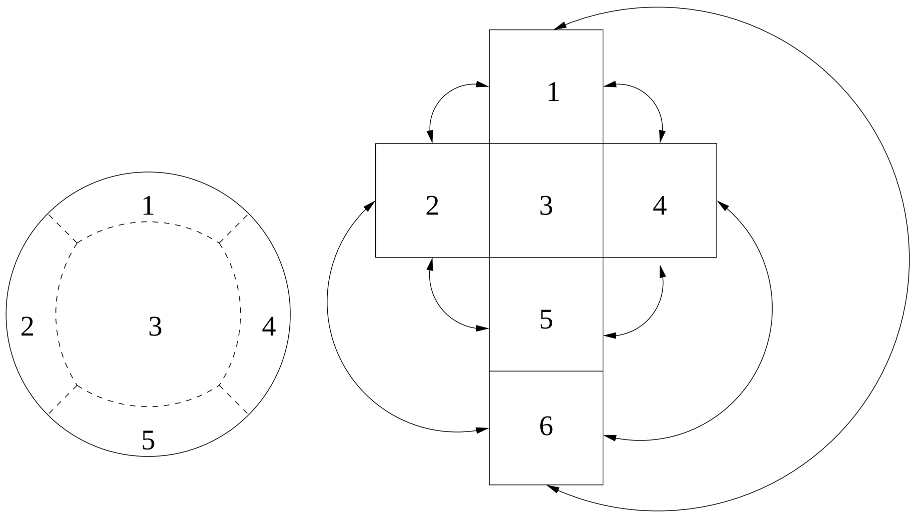

Figure 11: *The spherical cube, its projection onto 6 quadrants and how they are connected*

should be attached to the appropriate neighboring face, giving us a closed 2d body.

Recently, in his Ph.D.-thesis, J. Rossmanith [Ros02] has tried this grid for the SWE and successfully applied it to a problem similar to Test case 5 of Williamson et al. [WDH+91]. This path should definitely be pursued further. Other FVM-codes avoid the pole-problem by using spherical triangles [CHJJ96], taking as their initial discretization the icosahedron.

7 Conclusions and future work

Through this work we have confirmed that finite volume techniques is a candidate for solving flow problems on the sphere. In particular the technique should be seriously considered when conservation is important.

CLAWPACK proved to be quality software with appropriate documentation. But some effort is needed from the user to get a good solver. In particular it is the user's responsibility to provide a Riemann solver and the appropriate decomposition into waves. Choosing the right decomposition strategy turns out to be crucial for our problem and only the flux-based wave decomposition gave a satisfactory result.

Being on a sphere requires that a transformation to a computational grid is needed. Our simple choice of a global latitude-longitude grid proved to be insufficient. The first thing on our agenda is to try a better grid which does not gives artificial boundaries on the sphere.

We also plan to try adaptive mesh refinement. We believe this could be a great advantage when turbulence occurs locally, as it will in many cases when topography is introduced. A prime example is Test case 5 of the test suite.

References

[Alf97] P. Alfeld. *The Platonic Solids.* `http://www.math.utah.edu/~alfeld/math/polyhedra/polyhedra.html`, September 1997.

[BC84] M. J. Berger and P. Colella. Local Adaptive Mesh Refinement for Shock Hydrodynamics. *Journal of Computational Physics*, 53(3):561–568, 1984.

[Beh98] J. Behrens. Atmospheric and ocean modeling with an adaptive finite element solver for the shallow-water equations. *Applied Numerical Mathematics*, 26:217–226, 1998.

[BL97] M. J. Berger and R. J. LeVeque. AMRCLAW, Adaptive Mesh Refinement + CLAWPACK. `http://www.amath.washington.edu/~rjl/amrclaw`, 1997.

[BL98] M. J. Berger and R. J. LeVeque. Adaptive Mesh Refinement using Wave-Propagation Algorithms for Hyperbolic Systems. *SIAM Journal on Numerical Analysis*, 35(6):2298–2316, 1998.

[BLMR03] D. S. Bale, R. J. LeVeque, S. Mitran, and J. A. Rossmanith. A Wave Propagation Method for Conservation Laws and Balance Laws with Spatially-Varying Flux Functions. *SIAM Journal on Scientific Computing*, 24:955–978, 2003.

[BO84] M. J. Berger and J. Oliger. Adaptive Mesh Refinement for Hyperbolic Partial Differential Equations. *Journal of Computational Physics*, 53, 1984.

[CDMW98a] S. Chippada, C. N. Dawson, M. L. Martinez-Canales, and M. F. Wheeler. Finite Element Approximations to the System of Shallow Water Equations I: Continuous-Time A Priori Error Estimates. *SIAM Journal on Numerical Analysis*, 35(2):692–711, 1998.

[CDMW98b] S. Chippada, C. N. Dawson, M. L. Martinez-Canales, and M. F. Wheeler. Finite Element Approximations to the System of Shallow Water Equations, Part II: Discrete-Time A Priori Error Estimates. *SIAM Journal on Numerical Analysis*, 36(1):226–250, 1998.

[CHJJ96] K. Cassirer, R. Hess, C. Jablonowski, and W. Joppich. The shallow water test cases for a global model with documentation of the results. Technical report, GMD - German National Research Center for Information Technology, 53754 Sankt Augustin, 1996.

[CS90] J. Coté and A. Stanisforth. An accurate and efficient finite-element global model for the shallow-water primitive equations. *Monthly Weather Review*, 118:2707–2717, 1990.

[DM00] C. N. Dawson and M. L. Martinez-Canales. Finite Element Approximations to the System of Shallow Water Equations, Part III: On the Treatment of Boundary Conditions. *SIAM Journal on Numerical Analysis*, 38(1):149–159, 2000.

[EMR70] E. B. Eliassen, B. Machenhauer, and E. Rasmussen. On a numerical method for integration of the hydrodynamical equation with a spectral representation of the horizontal fields. Technical report, Institut for teoretisk Meteorologi, University of Copenhagen, 1970.

[Gat92] W. Lawrence Gates. AMIP: The atmospheric model intercomparison project. *Bulletin of the American Meteorological Society*, 73(12), 1992.

[Gro73] G. Grotkop. Finite element analysis of long period water waves. *Computer Methods in Applied Mechanics and Engineering*, 2(148), 1973.

[Hei02] T. Heinze. The shallow water equations on the sphere and their Lagrange-Galerkin-solution. *Meteorology and Atmospheric Physics*, 81(1):129–135, 2002.

[HH83] A. Harten and J. M. Hyman. Self-adjusting grid methods for one-dimensional hyperbolic conservation laws. *Journal of Computational Physics*, 50:235–269, 1983.

[JCHW95] R. Jakob-Chien, J. J. Hack, and D. L. Williamson. Spectral transform solution to the shallow water test set. *Journal of Computational Physics*, 119(1):164–187, 1995.

[LeV02] R. J. LeVeque. *Finite Volume Methods for Hyperbolic Problems.* Cambridge University Press, 2002.

[LLBM00] R. J. LeVeque, J. O. Langseth, M. J. Berger, and S. Mitran. CLAWPACK 4.0, a Software Package for Conservation Laws and Hyperbolic Systems. `http://www.amath.washington.edu/claw`, 2000.

[Orz70] S. A. Orzag. Transform method for calculation of vector coupled sums: Application to the spectral form of the vorticity equation. *Journal of the Atmospheric Sciences*, 27:890–895, 1970.

[Roe81] P. L. Roe. Approximate Riemann Solvers, Parameter Vectors, and Difference Schemes. *Journal of Computational Physics*, 43:357–372, 1981.

[Ros02] J. A. Rossmanith. *A Wave Propagation Method with Constrained Transport for Ideal and Shallow Water Magnetohydrodynamics*. PhD thesis, Applied Mathematics, University of Washington, 2002.

[Str68] G. Strang. On the construction and comparison of difference scheme. *SIAM Journal of Numerical Analysis*, 5:506–517, 1968.

[Swa00] P. N. Swarztrauber. Spectral transform methods for solving the shallow water equations on the sphere. *Monthly Weather Review*, 124:730–744, 2000.

[TTI97] M. Taylor, J. Tribbia, and M. Iskandarani. The spectral element method for the shallow water equations on the sphere. *Journal of Computational Physics*, 130(1):92–108, 1997.

[vL77] B. van Leer. Towards the ultimate conservative difference scheme iv. a new approavh to numerical convection. *Journal of Computational Physics*, 23:276–299, 1977.

[WDH+91] D. L. Williamson, J. B. Drake, J. J. Hack, R. Jakob, and P. N. Swarztrauber. A Standard Test Set for Numerical Approximations to the Shallow Water Equations in Spherical Geometry. *Journal of Computational Physics*, 102(1):211–224, 1991.